PLOS ONE

Human pericytes degrade diverse α-synuclein aggregates

Birger Victor Dieriks[1,2]*, Blake Highet[1,2], Ania Alik[3], Tracy Bellande[3], Taylor J. Stevenson[1,2], Victoria Low[1,2], Thomas I-H Park[2,4], Jason Correia[2,5], Patrick Schweder[2,5], Richard L. M. Faull[1,2], Ronald Melki[3], Maurice A. Curtis[1,2], Mike Dragunow[2,4]*

1 Department of Anatomy and Medical Imaging, University of Auckland, Auckland, New Zealand, 2 Centre for Brain Research, University of Auckland, Auckland, New Zealand, 3 Molecular Imaging Research Center, Francois Jacob Institute, Alternative Energies and Atomic Energy Commission, and Laboratory of Neurodegenerative Diseases, National Center for Scientific Research, Fontenay- Aux-Roses, France, 4 Department of Pharmacology, University of Auckland, Auckland, New Zealand, 5 Auckland City Hospital, Auckland, New Zealand

* v.dieriks@auckland.ac.nz (BVD); m.dragunow@auckland.ac.nz (MD)

Abstract

Parkinson's disease (PD) is a progressive, neurodegenerative disorder characterised by the abnormal accumulation of α-synuclein (α-syn) aggregates. Central to disease progression is the gradual spread of pathological α-syn. α-syn aggregation is closely linked to progressive neuron loss. As such, clearance of α-syn aggregates may slow the progression of PD and lead to less severe symptoms. Evidence is increasing that non-neuronal cells play a role in PD and other synucleinopathies such as Lewy body dementia and multiple system atrophy. Our previous work has shown that pericytes—vascular mural cells that regulate the blood-brain barrier—contain α-syn aggregates in human PD brains. Here, we demonstrate that pericytes efficiently internalise fibrillar α-syn irrespective of being in a monoculture or mixed neuronal cell culture. Pericytes cleave fibrillar α-syn aggregates (Fibrils, Ribbons, fibrils65, fibrils91 and fibrils110), with cleaved α-syn remaining present for up to 21 days. The number of α-syn aggregates/cell and average aggregate size depends on the type of strain, but differences disappear within 5 five hours of treatment. Our results highlight the role brain vasculature may play in reducing α-syn aggregate burden in PD.

Introduction

Parkinson's disease (PD) is a progressive, degenerative disorder of the brain that primarily affects the dopaminergic neurons in the substantia nigra and causes characteristic movement symptoms. Pathologically, PD is grouped with other synucleinopathies such as Lewy body dementia (LBD) and multiple system atrophy (MSA), which are all characterised by the abnormal accumulation of α-synuclein (α-syn) aggregates. Current data suggests that under normal physiological circumstances, monomeric cytosolic α-syn exists in a transient state until the protein interacts with membranes, where it plays a role in synaptic transmission, vesicle endocytosis and membrane remodeling [1]. However, in people with PD, an event takes place that

allows the formation of an initial α-syn oligomer or aggregate [2]. Once an initial α-syn oligomer is established, the oligomer functions as a seed to form larger and more extensive aggregates such as Lewy bodies and Lewy neurites. This aggregate formation process is important in α-syn pathogenicity and progressive neurodegeneration in PD [2]. In most instances, cells can break down these aggregates through macroautophagy, chaperone and proteasome machinery (reviewed in [3]). However, progressive α-syn aggregation may exceed the clearance capacity of affected cells. Aging further reduces these protective mechanisms, enhancing aggregate accumulation and spreading to neighbouring cells, where the process is repeated. Over several years α-syn aggregates slowly spread into other brain regions, causing the gradual onset of characteristic PD symptoms [2,4].

This mode of action explains the gradual onset of disease but does not explain the variability in cell types affected and symptoms observed in patients with PD, LBD and MSA [5]. Several studies have identified noticeable differences in structural and phenotypic traits of fibrillar α-syn aggregates concerning seeding capacity and neurotoxicity. This led to the hypothesis that different α-syn aggregate 3D conformations or 'strains' may be partly responsible for the heterogeneous nature of PD and other synucleinopathies [6,7]. Several studies show that injection of pure α-syn strains or brain extracts isolated directly from human PD and other synucleinopathies into the rodent brain results in differential cortical propagation of α-syn pathology and reproduces the heterogeneity in pathology and symptoms observed in the original patients. The structure of injected strains remains unchanged throughout this process, emphasising the link between strain and patient symptomatology [7–10].

Neurons are the primary source of endogenous α-syn within the brain, and in PD, many develop large α-syn aggregates or Lewy bodies. However, non-neuronal cells have become increasingly linked to PD, with α-syn aggregates found in astrocytes and microglia [11,12]. Our recent quantification study of human PD olfactory bulbs shows that the number of non-neuronal cells (including astrocytes, microglia and pericytes) containing small aggregates is similar to the number of neurons with small aggregates [13]. Astrocytes and microglia are involved in phagocytic clearance of α-syn in a coordinated attempt to avoid propagation of PD pathology to neighbouring neurons [14–16]. However, nothing is known about the potential α-syn clearance role of pericytes in the brain.

Pericytes are contractile cells that regulate blood flow and permeability of the blood-brain barrier. Pericytes play an important role in neuroinflammation, acting as targets and early initiators of brain inflammation in response to systemic inflammation before astrocyte and microglia activation [17–19]. PD causes loss of pericyte coverage of vessels and leakiness of the blood-brain barrier [20,21]. Furthermore, pericytes overexpressing α-syn in the cytoplasm can transfer α-syn through nanotubes that connect neighbouring cells, as the observed exchange between neurons and astrocytes [22–24]. Like microglia and astrocytes, pericytes could contribute a neuroprotective role in the clearance of α-syn aggregates, thereby reducing α-syn-induced toxicity in neurons and slowing down spread [14,15]. Therefore, we studied pericyte α-syn degradation by exposing cultured primary human pericytes to various fibrillar α-syn aggregates and measured if degradation was impaired in PD pericytes. Our results may inform whether targeting pericyte degradation of α-syn is a useful therapeutic option.

Materials & methods

Study design

In this study, we used different α-syn antibodies to study α-syn aggregates in pericytes derived from control and PD post-mortem brains. Pericytes were exposed for four hours to five distinct α-syn aggregates (Fibrils, Ribbons, fibrils65, fibrils91 and fibrils110). α-syn degradation

and abundance were measured via western blot and fluorescence microscopy for up to 21 days.

Alpha-synuclein fibril generation

Human wild-type monomeric α-syn was expressed in E. coli BL21 DE3 CodonPlus cells (Agilent Technologies) and purified as described previously [25]. To assemble human wild-type α-syn into the different fibrillar aggregates, the full-length monomeric protein (250μM) was incubated in 50 mM Tris–HCl, pH 7.5, 150 mM KCl for "fibrils"; in 5 mM Tris–HCl, pH 7.5 for "ribbons"; in 20mM MES pH 6.5 for "fibrils65" and 20mM KPO4, 150mM KCl for "fibrils91" at 37˚C under continuous shaking in an Eppendorf Thermomixer set at 600 r.p.m for seven days [26,27]. A human α-syn lacking 30 C-terminal amino-acid residues, α-syn 1–110 was generated by introducing two stop codons after residue 110 by site-directed mutagenesis. This variant was purified as full-length -syn and assembled into fibrillar structures "fibrils110" in 50 mM Tris–HCl, pH 7.5, 150 mM KCl. The assembly reaction was followed by withdrawing aliquots (10 μl) from the assembly reaction at different time intervals, mixing them with Thioflavin T (400μl, 10 μM final) and recording the fluorescence increase on a Cary Eclipse Fluorescence Spectrophotometer (Varian Medical Systems Inc.) using an excitation wavelength = 440 nm, an emission wavelength = 480 nm and excitation and emission slits set at 5 and 10 nm, respectively. Following assembly reaction, fibrils were fragmented to an average length of 42–52 nm by sonication for 20 min in 2 mL Eppendorf tubes in a Vial Tweeter powered by an ultrasonic processor UIS250v (250 W, 2.4 kHz; Hielscher Ultrasonic, Fig 1A). The molecular mass of fragmented fibrils was then determined by analytical ultracentrifugation [28]. Fibrils were made on average of 8300 monomers, which means that a working concentration of 2 μM equivalent monomeric α-syn corresponds to a particles (fibrils) concentration of 0.24 nM (2000/8300 = 0.24). All α-syn preparations were quantified for endotoxin levels as described previously [8,29] to prove that endotoxin levels were below 0.02 endotoxin units/mg (EU/mg) using the Pierce LAL Chromogenic Endotoxin Quantification Kit.

To label α-syn fibrils with extrinsic fluorophores, the fibrils were centrifuged twice at 15,000g for 10 min and re-suspended twice in PBS at 100μM, and two molar equivalents of ATTO-488 NHS-ester or ATTO-647 NHS-ester (#AD 488–35 and #AD 647–35, Atto-Tec GmbH) fluorophore in DMSO were added. The mix was incubated for 1 h at room temperature. The labelling reactions were arrested by the addition of 1mM Tris pH 7.5. The unreacted fluorophore was removed by a final cycle of two centrifugations at 15,000 g for 10 min and resuspensions of the pellets in PBS. Transmission Electron Microscopy (TEM) assessed the fibrillar nature of a-syn after adsorption of the fibrils onto carbon-coated 200 mesh grids and negative staining with 1% uranyl acetate using a Jeol 1400 transmission electron microscope (Fig 1).

The images were recorded with a Gatan Orius CCD camera (Gatan, Pleasanton). The resulting α-syn fibrils were fragmented by sonication for 20 min in 2 mL Eppendorf tubes in a Vial Tweeter powered by an ultrasonic processor UIS250v (250 W, 2.4 kHz; Hielscher Ultrasonic) to generate fibrillar particles with an average size 42–52 nm as assessed by TEM analysis.

Human brain tissue

This study's post-mortem adult human brain tissue was obtained from the Neurological Foundation Human Brain Bank (Centre for Brain Research, University of Auckland). The University of Auckland Human Participants Ethics Committee approved the protocols used in these studies (approval# 011654). The Health and Disabilities Ethics Committee New Zealand
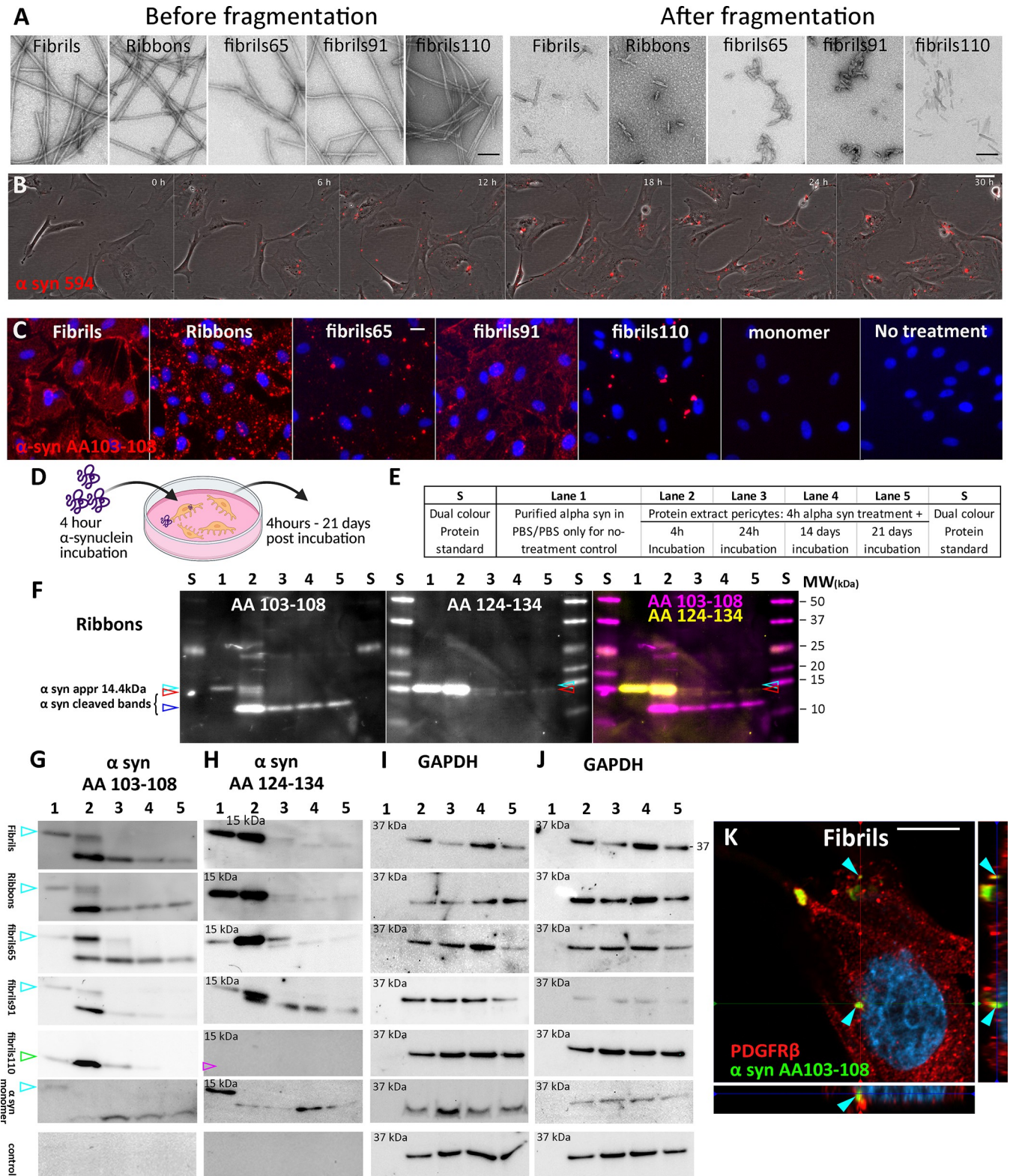
Fig 1. Internalisation and degradation of α-syn strains in pericytes. (A) Electron microscopy of α-syn strains before and after fragmentation. (B) Live cell imaging of fluorescently tagged α-syn for 30 hours. (C) Immunofluorescent labelling of α-syn strains after 30 min in control pericytes with α-syn epitope-specific antibody AA103-108. (D) Schematic representation of experimental setup. (E) Loading of western blots. Lane 1 only contains pure α-syn aggregate, whereas lane 2–5 shows α-syn isolated from pericytes. (F) Detailed fluorescent western blot with α-syn epitope-specific antibodies detecting Ribbons with α-

syn antibody AA103-108 (magenta), AA124-134 (yellow) and merge showing overlap of α-syn bands. Various bands are identified indicating full length (14.4kDa, cyan arrow) and cleaved α-syn (red and blue arrows). α-syn detection on individual western blots for Fibrils, Ribbons, fibrils65, fibrils91, fibrils110 and no-treatment control (PBS) with α-syn epitope specific antibodies showing full length α-syn (cyan arrow) and cleaved α-syn fragments. Fibrils110 lacks a full-length band as aggregate is made up of C-term cleaved α-syn (green arrow). (G) AA 103–108, (H) AA124-134, and (H) GAPDH blot corresponds to blot shown in G after antibody stripping and relabelling. Full blots shown in S1 Raw images. Confocal image with orthogonal views showing pericyte with internalised α-syn Fibrils after 24 hours (cyan arrows, K). Scale bars represent 100 nm (A), 20 μm (B,C), 10 μm (K).

https://doi.org/10.1371/journal.pone.0277658.g001

approved the use of surgically removed brain tissue (biopsy tissue approval# AKL/88/025). Written, informed consent was obtained from the individual(s) and/or next of kin to use the tissue. Pathological assessment of neurologically normal cases (controls) reported no disease-related pathology beyond that expected in aged individuals, and all PD cases were confirmed by a neuropathologist (Table 1). The PMD and age of death in PD vs control brain pericyte donors differed (control PMD:18.4 ± 4.0, age: 50.6 ±11.2; PD PMD: 4.3 ± 1.8, age: 77 ± 8.9). For this reason, PD and control pericytes (n = 3 in each group) were analysed separately. The neurosurgical brain tissue was obtained with written informed consent from Auckland City Hospital under HDEC ethics approval AKL/88/025.

Isolation of primary human brain pericytes

Middle temporal gyrus (MTG) tissue was used to generate pericyte cultures from human post-mortem brains with a PD diagnosis or pathologically normal (control) cases as determined by a neuropathologist (Table 1). We found that post-mortem delay (PMD) had less effect on the viability of pericyte cultures compared to the age at death and disease diagnosis. Viable pericytes can be grown from brain tissue up to 48 hours post-mortem. A detailed description of generating pericyte cultures by our group has previously been described [19,30]. In short, MTG tissue was mechanically dissected and dissociated before enzymatic digestion in Hank's balanced salt solution (HBSS), containing 2.5 U/mL papain (Worthington) and 100 U/mL DNase 1 (ThermoFisher) for 30 minutes at 37˚C with gentle rotation. This step included a gentle titration at 15 minutes. Following this, complete media, DMEM: F12 (ThermoFisher), was used to stop the enzymatic digestion. To collect the cells, they were centrifuged (170g, 10 min) and re-suspended in complete media. Cells were plated onto uncoated T75 culture flasks

Table 1. Case information for post-mortem and surgical removedbrain tissue used in this study.

Case	diagnosis	Brain region	age (years)	Sex	PMD (hours)	brain weight (g)	cause of death	duration of PD (years)	Cell types used
H189	control	MTG	41	M	16	1412	Asphyxia	/	pericytes
H209	control	MTG	48	M	23	1470	Ischaemic heart disease	/	pericytes
H238	control	MTG	63	F	16	1324	Dissecting aortic aneurysm	/	pericytes
PD52	PD/CLBD	MTG	84	M	5	1067	Myocardial infarction	12	pericytes
PD65	PD/CLBD	MTG	67	M	2.25	1033.1	Parkinson's disease	9	pericytes
PD78	PD/CLBD	MTG	80	M	5.5	/	Parkinson's disease	7.5	pericytes
E212	Intractable Epilepsy	Temporal lobe	40	M	< 30 min	NA	NA	NA	Mixed neuronal cells
E213	Intractable Epilepsy	Temporal lobe	23	F	< 30 min	NA	NA	NA	Pericytes & mixed neuronal cells
E215	Intractable Epilepsy	Temporal lobe	29	F	< 30 min	NA	NA	NA	Mixed neuronal cells
T157	Cortical Dysplasia type IIB	Frontal Lobe	30	F	< 30 min	NA	NA	NA	Mixed neuronal cells

https://doi.org/10.1371/journal.pone.0277658.t001

(Nunc). Cells were subsequently incubated at 37˚C with 5% carbon dioxide until seeded for experiments, grown in DMEM:F12 (v) containing 10% foetal bovine serum (ThermoFisher) and 1% Penicillin/Streptomycin (ThermoFisher). For all the experiments presented here, pericytes were at passages 5–9. This ensures pure pericyte cultures without contamination of astrocytes or microglia. Late passages (> P4) displayed immunocytochemical staining for pericyte markers, including PDGFRβ, neural/glial antigen 2 (NG2), CD13, CD146 and desmin, which corresponds to the expression profile of human brains, capillary-associated pericytes [31]. Pericytes grown in these culture conditions have been well characterized, carry a unique inflammatory profile, and can phagocytose large beads [17,19,30–34].

Cell plating and incubation with α-syn aggregates

Cells were harvested for experiments by adding 2 mL 0.25% Trypsin-1mM ethylenediamine-tetraacetic acid (EDTA; ThermoFisher) and incubated for 2–5 minutes at 37˚C to allow for cell detachment. Cells were collected in warm DMEM: F12 media. 10 μL of 1:1 Trypan Blue (ThermoFisher) and the cell suspension was prepared and added to a haemocytometer for cell counting. Cells were re-suspended in the correct volume of DMEM: F12 to achieve the required cell density of 5,000 cells/well in 96-well plates (Nunc) or 50,000 cells in 6 well plates. Pericytes were treated at 37˚C with the various α-syn aggregates (Fibrils, Ribbons, fibrils65, fibrils91 or C-terminus truncated fibrils110, 100 nM in PBS) or PBS (no treatment control) for 4 hours, washed and subsequently returned at 37˚C until endpoint (0 hours– 37 days). Results up to 21 days are shown in this manuscript as no distinctive changes were observed between 21–37 days.

Primary mixed neuronal cultures

Grey matter isolated from normal cortex was mechanically dissociated into <1 mm pieces, followed by enzymatic digestion. Cells were grown in neuronal growth medium (DMEM: F12, supplemented with 2% B27, Penicillin/Streptomycin, GlutaMAX®, (ThermoFisher) 10 μM Y-27632 2HCl (Selleckchem); 2 μg Heparin (Sigma), 40 ng/ml of NGF, BDNF, NT-3, GDNF, and IGF-1 (Peprotech), plated onto poly-D-lysine (100μg/ml) coated coverslips and incubated at 37˚C with 5% CO_2. The culture media was half changed every 24 hours for the first 2 days and every 3–4 days after that. These cultures are extensively characterised and contain a mixture of neurons with mature neurophysiological properties, astrocytes, pericytes and microglia [35].

Live-cell imaging

Pericytes, cultured in small Petri dishes (150318, Nunc, ThermoFisher), were treated with 100nM α-syn-atto 647 for 4h, washed and placed in a Nikon Biostation cell incubator (5% CO_2, 37˚C, Plan Fluor 20x/ 0.5 NA DL) for up to 120 h. Images of brain pericytes were captured every 5 min during this period. During imaging, no readily identifiable adverse phototoxic effects were observed on the cells.

Protein isolation and western blotting

Whole pericytes cell lysate was rinsed with ice-cold PBS and isolated at the endpoint from 6 well plates with 100μl sample harvesting buffer (62.5 mM Tris-HCl pH 6.8, 2% SDS, 10% glycerol). Cells were scraped off, boiled at 100˚C for 10 min, and the lysate was stored at-80˚C. Western blot was performed according to the manufacturer guidelines using Novex 10–20% Tris-Glycine Mini Gels (XP10202BOX, ThermoFisher). Proteins were subsequently

electrotransferred onto a polyvinylidene difluoride membrane (PVDF, Hybond-P; Amersham) using Novex Tris-Glycine Native Running Buffer in a BioRad blot module. For immuno-staining, the membrane was blocked for one hour using Odyssey blocking buffer/TBS-T (1:1; 0.1% Triton-X). Primary antibodies were incubated overnight at 4˚C in Odyssey blocking buffer/ TBS-T (1:1). Antibodies raised against α-syn C-terminus (Mouse anti α-syn, Amino Acid (AA) 124–134 (1:1,000) and ab1903 (Abcam); Mouse anti α-syn 4B12, AA 103–108, IgG1 (1:2,000, MA1-90346, ThermoFisher), GAPDH (1:1,000, ab9484, Abcam). Blots were washed in TBS-T and incubated with fluorescently conjugated secondary antibodies for 3 hours at room temperature in Odyssey blocking buffer/TBS-T (1:1 and 0.02% SDS; IRDye 800CW Donkey anti-mouse, 926–32212 (Li-COR)). Blots were washed (3 x 5min TBS-T and 2 x 5 min TBS) before being imaged on the ChemiDoc MP Imaging System (Biorad). Subsequently, gels were stripped for 30 min at 60˚C (62.5 nM Tris, pH6.8; 2%SDS; 100 mM β-mercaptoethanol), extensively washed in TBS-T before being re-probed for GAPDH. For these experiments, the samples were run on two gels, with the first blot labelled with AA103-108 and the second blot labelled with AA124-134. After imaging both gels, they were stripped and relabelled for GAPDH. Full western blots are available in (S1 Raw images).

Immunocytochemistry

At endpoints, cells were fixed in 4% paraformaldehyde for 15 min and washed/permeabilised with phosphate buffered saline (PBS) with 0.2% Triton X-100TM (PBS-T). Cells were incubated overnight at 4˚C with primary antibodies—targeting α-syn (Mouse anti α-syn, AA 124–134, ab1903, Abcam; Mouse anti α-syn 4B12, AA 103–108, IgG1, MA1-90346, ThermoFisher; pericytes (Rabbit anti-PDGFR β, ab32570, Abcam; gt PDGFR β, AF-385, R&D systems)— diluted in immunobuffer (1% goat or donkey serum, 0.2% Triton X-100 in PBS). Cells were rewashed in PBS-T and incubated with filtered (0.22 μm syringe filter, Merck) fluorescently conjugated secondary antibodies and 20 μM Hoechst 33258 (ThermoFisher) for 2 hours at room temperature. Images were acquired using the automated fluorescence microscope ImageXpress® Micro XLS (Version 5.3.0.1, Molecular Devices) using the 20 x (0.45 NA) CFI Super Plan Fluor ELWD ADM objective lens and Lumencor Spectra X configurable light engine source. Confocal images were acquired using a LSM 800 Airyscan confocal microscope (Zeiss LSM 800 Airyscan confocal microscope) with a 40x/1.3 or 63x/1.4 NA Plan Apochromat oil immersion using the Airyscan module.

High content image analysis

Images acquired on the ImageXpress® Micro XLS at respective endpoints were exported from MetaXpress (software information) as uncompressed 16-bit TIFFs for analysis using FIJI (version #1.52p). A rolling-ball median filter (radius = 2.0 pixels) was applied to Hoechst images for background subtraction before running "Find Maxima" to define cell boundaries using Voronoi tessellation (prominence = 500). Cell boundaries were then added to the region of interest (ROI) manager, excluding cells on edges of image frames. Cell nuclei were then auto-threshold masked using the 'Huang' setting to find the cell nucleus area. Next, the α-syn images (AA103-108) were processed by applying a median (radius = 2.0) and Gaussian filter (sigma = 15.0) to duplicates of the image before subtracting the gaussian processed image from the median processed image to reduce noise and identify background, respectively. The resulting images were thresholded (82, 65535) using the 'Default' method before converting to a binary mask. These masks were then counted, with a minimum aggregate size of 2 pixels^2. For intensity measurements, intensity measurements within cell masks were made on raw

aggregate images. This process was batch processed on the entire image set using a custom
ImageJ macro. The script for this analysis is available in supplementary information.

Immunohistochemistry

For the immunohistochemical studies, the human brains were processed and labelled as previ-
ously described [24,36,37]. 7 μm-thick sections from paraffin-embedded MTG blocks were cut
using a rotary microtome (Leica Biosystems RM2235) and mounted onto Über plus printer
slides (InstrumeC) in a water bath set to 42˚C (Leica Biosystems H1210). Sections were left to
dry for 72 hours at room temperature prior to immunohistochemical staining.

Sections were then blocked in 10% normal goat serum in PBS for 1 hour at RT. Subse-
quently, the sections were incubated with primary antibodies (α-synuclein-phospho S129,
ab51253, Abcam) overnight at 4˚C. Sections were incubated with the corresponding goat sec-
ondary Alexa Fluor (488, 594, 647) conjugated secondary antibody (ThermoFisher) and
Hoechst 33342 (Thermofisher) at 1:500 for 3 hours at RT. Control sections where the primary
antibody was omitted showed no immunoreactivity. The control experiments showed that the
secondary antibodies displayed no cross-reactivity. Fluorescent images were captured with a
MetaSystems VSlide slide scanner with a 20x dry lens (NA 0.9).

Data visualisation and statistical hypothesis

Data visualisation and statistical hypothesis testing were performed using GraphPad Prism®
Version 9.00 and R Version 4.0. The colours represent a 2D kernel density estimation. It is
scaled to 1 for each graph, with the bright yellow area displaying the highest density of cells.
All experiments were performed in at least three independent cases. In general, data are
expressed as individual cells or average/case. Data visualisation and statistical hypothesis test-
ing were performed using GraphPad Prism® Version 7.00. Two-way analysis of variance
(ANOVA) was used when comparing responses across a number of stimuli with Tukey's post
hoc adjustment for multiple comparisons. One-way analysis of variance (ANOVA) was used
when comparing across cell types with Tukey's multiple comparison adjustment. Linear
regression was used to analyse correlations. Statistical significance was set at $p < 0.05$. Final
figures were composed using Adobe Photoshop CC (Adobe Systems Incorporated, v20.0.6).

Results

α-syn aggregates are internalised and cleaved by pericytes

Live cell imaging showed rapid uptake of various fibrillar α-syn aggregates (Fibrils, Ribbons,
fibrils65, fibrils91 or fibrils110) in pericytes when added to the culture media. α-syn formed
discrete spots within the pericytes (Fig 1B) in agreement with what we reported using astro-
cytes induced from human pluripotent stem cells [16]. Binding and internalisation of fibrillar
α-syn aggregates revealed apparent visual differences observed within 30 min after treatment
in agreement with what we reported for rodent neurons [38]. Fibrils and fibrils91 are primarily
found membrane-bound on the pericytes. As uptake progressed, this distribution gradually
changed to a punctate pattern, whereas Ribbons, fibrils65 and fibrils110 already showed a
punctate pattern. 30 min after adding fibrillar α-syn, all cells within the culture displayed posi-
tive α-syn labelling except fibrils110, where only a subset of cells contained α-syn. No puncta
were observed in pericytes treated with monomeric α-syn (Figs 1C and S1B).

Pericytes were subsequently incubated with each of the five α-syn aggregates (Fibrils, Rib-
bons, fibrils65, fibrils91 or fibrils110) to test their ability to degrade α-syn (experimental setup,
Fig 1D). Pericytes were pre-treated with fibrillar α-syn for 4 hours before excess α-syn was

washed off and followed for an additional 4 hours—21 days Two antibodies directed against the C- terminal part of α-syn (AA103-108 and AA124-134) clearly labelled exogenous α-syn (before addition to cells). For western blot gel layouts, refer to Fig 1E. Protein extracts from pericytes exposed to α-syn (Ribbons) showed immunoreactivity at approximately 14 kDa and two lower bands bearing AA103-108 (white, Fig 1F); and 14kDa and one lower band bearing AA124-134 (magenta; Fig 1F). Full length α-syn (14 kDa) was no longer visible after 14 days. On the contrary cleaved α-syn bands remained visible up to 21 days with AA103-108 and AA124-134.

When comparing the five α-syn aggregates, we observed a similar pattern for Fibrils, Ribbons, fibrils65 and fibrils91 (Fig 1G and 1H; GAPDH bands for each blot Fig 1I and 1J). Full length α-syn was observed up to 24 hours (cyan arrow), and cleaved α-syn was seen until 21 days. Because fibrils110 is comprised of C-terminus truncated protein, we only observed a lower α-syn band (green arrow) corresponding to the cleaved fragment observed in the other α-syn aggregates when labelled with AA103-108 (Fig 1G). AA103-108 detected fibrils110 (Fig 1G), whereas AA124-134 did not (magenta arrow, Fig 1I and 1H), confirming that the C-terminus portion was lacking from fibrils110. No α-syn bands were present in the untreated control (bottom panel: Fig 1G–1I). These results indicate that pericytes have low or do not have endogenous α-syn, but they can internalise and process α-syn aggregates into discretely sized fragments. Western blotting could not detect full-length α-syn after 24 hours, whereas cleaved α-syn remained present within pericytes for up to 21 days. These findings show that AA103-108 and AA124-134 detect full-length α-syn. Two different α-syn bands are identified by AA103-108 and AA124-134, indicating that pericytes cleave α-syn at two different cleavage sites. AA103-108 was the only antibody consistently identifying cleaved α-syn for all α-syn aggregates.

α-syn was immunolabelled within pericytes using the AA103-108 antibody that enables detection of internalised full-length and cleaved fibrillar α-syn (cyan arrows show internalised α-syn fibrils; Fig 1K). Monomeric α-syn was not included in this time course as no α-syn puncta were observed (S1A Fig).

When qualitatively comparing uptake five hours after treatment, Fibrils, Ribbons, and fibrils91 showed a similar pattern of punctate aggregates of different sizes (Fig 2A–2F). Fibrils65 had a similar pattern, with fewer overall aggregates identified. However, larger aggregates were occasionally visualised (magenta arrow). The biggest differences were observed between fibrils110 and the other α-syn aggregates. Fibrils110 had a low number of highly immunoreactive aggregates per cell, with several cells devoid of aggregates (white arrow). Despite the large variability observed between cells treated, some general observations were apparent. Fibrils, Ribbons and fibrils91 displayed immunoreactivity for many small aggregates in most cells, whereas pericytes treated with fibrils110 displayed a small number of large immunoreactive aggregates in a small proportion of cells (Fig 2A–2F). This agrees with our previous observations using these α-syn aggregates and astrocytes induced from human pluripotent stem cells [16]. No phosphorylated α-syn was observed at any timepoint (S1B–S1C Fig).

Live cell imaging of the α-syn aggregates further confirmed these observations. Throughout the recordings, pericytes frequently underwent mitosis, indicating that internalised fluorescently tagged α-syn aggregates do not inhibit cell division (see S1–S5 Movies).

3D Confocal Airyscan images of pericytes labelled with PDGFRβ (red) treated with α-syn aggregates confirmed previous observations at 5 hours with AA103-108. After five days α-syn was present in the form of punctate aggregates (orange arrows) and elongated fibres (white arrows; Fig 2G–2P).
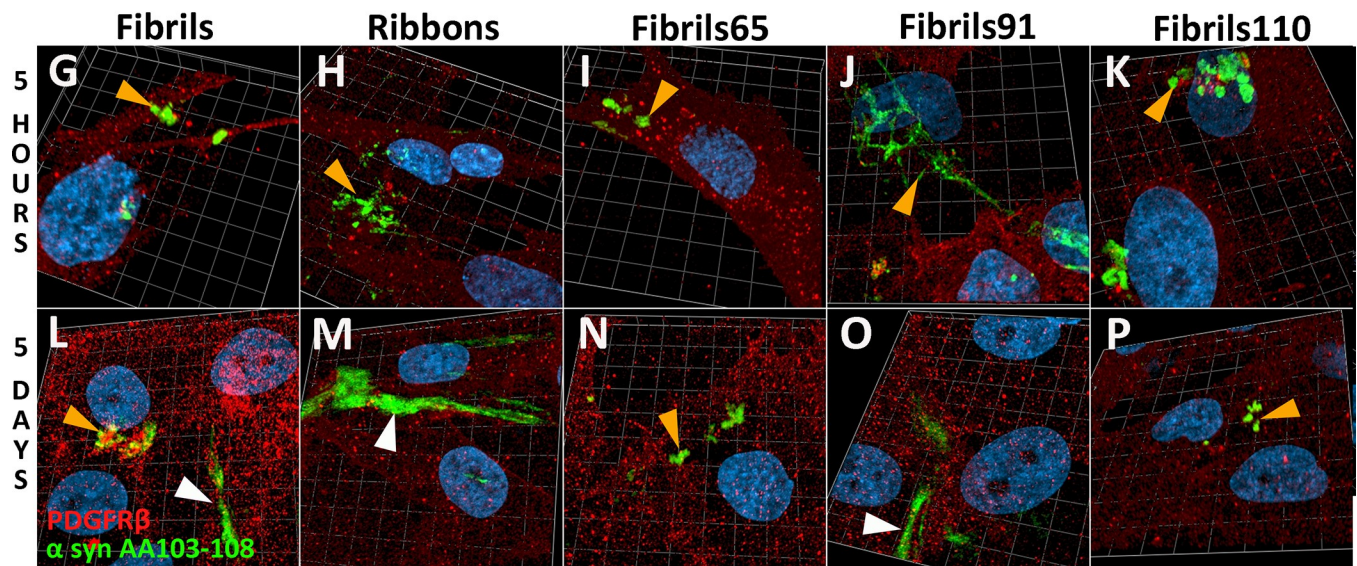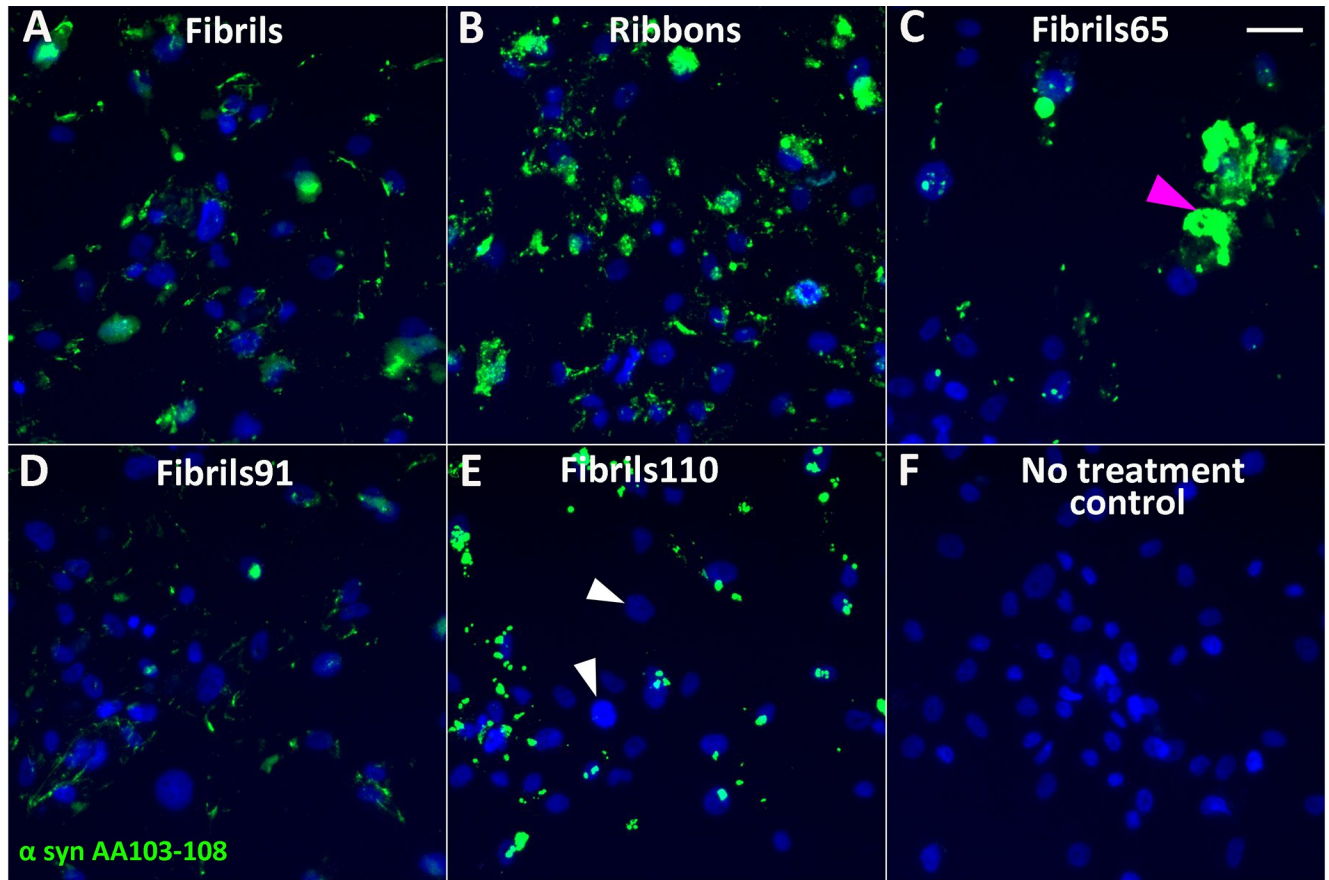
Fig 2. Immunofluorescent labelling of α-syn strains in control pericytes with α-syn epitope-specific antibodies AA103-108 (green). Strains specific fluorescent staining 5 hours after pre-treatment with 100nM α-syn. At early time point, all cells contain aggregates, except for fibrils110 treated cells (white arrows); (A) Fibrils, (B) Ribbons, (C) fibrils65, with occasional larger aggregates (magenta arrow), (D) fibrils91, (E) fibrils110, (F) no treatment control. 3D confocal view of α-syn aggregates in pericytes 5 hours and 5 days after pre-treatment with 100nM (D, I) Fibrils, (E, J) Ribbons, (F, J) fibrils65, (G, K) fibrils91, (H, L) fibrils110. Typically aggregates appear as spots (orange arrows) with thicker fibres (white arrows) appearing more frequently at later time points. Scale bars represent 50 μm.

Clearance of aggregated α-syn in pericytes derived from control and PD patients

Following pre-treatment with α-syn aggregates (4 hours, 100nM), pericytes fixed at seven time-points (0–21 days) were labelled with AA103-108 antibody. α-syn aggregate density gradually decreased over time with α-syn AA103-108 remaining visible up to 21 days. α-syn was present in the form of punctate aggregates and elongated fibres (green arrows, Fig 3). As described above, fibrils65 occasionally displayed large, intense α-syn aggregates (magenta arrow). These large fibrils65 puncta are a visualisation artifact caused by representing all the α-syn aggregates with the same brightness settings. Subsequent analysis of the raw data showed that these large fibrils65 puncta comprise several individual aggregates. The untreated control showed no α-syn immunolabelling (Fig 3). This labelling validated our western blot data while including additional time points.

To assess α-syn aggregate clearance in pericytes, automated quantification of aggregated α-syn detected with AA103-108 antibodies in single cells was conducted (Fig 4). We analysed control (n = 3) and PD-derived (n = 3) pericytes separately as they displayed differences in PMD delay and age of death. Differences were limited to the earliest time points, therefor we only presented data from the first 24 hours. Even though individual pericytes revealed variation in the average aggregate size/cell and average aggregate count/cell for each strain type, the mean values for each case are a good representation of our observations. At 0 hours, there were significantly more aggregates/cell for Fibrils and Ribbons compared to fibrils65 and fibrils110 in both control and PD pericytes. This difference remained up to 5 hours in the PD pericytes (Fig 4A and 4B). The average aggregate size for Fibrils was higher at 0 hours compared to Ribbons and fibrils91(Fig 4C and 4D).

Combined representation of aggregate counts and average aggregate size for each cell as density plots showed greater variability in PD-derived compared to control pericytes for all strain types. The vertical bars represent the fraction of cells with aggregates (Fig 5). For Ribbons, most control pericytes contained a small number of small aggregates (up to 10 counts/cell, colours yellow to purple on the plot). The aggregate counts spread in PD-derived pericytes went up to 28 counts/cell while maintaining the same aggregate size range. Immediately after exposing pericytes to Ribbons, at time 0h, the proportion of pericytes containing aggregates from control and PD was 94.4 and 99.5%, respectively. On day 14, the proportion of pericytes containing aggregates from control and PD decreased to 57.5 and 59.3%, respectively, indicating that a high proportion of pericytes still had α-syn aggregates (Fig 5A). For fibrils110, control pericytes displayed limited variation with most cells containing 1–5 aggregates, while that varied more in PD pericytes (up to 10 counts/cell). The number of cells containing aggregates differed markedly upon exposing pericytes to fibrils110. A large proportion of control pericytes were devoid of aggregates at 0h (43% for controls, 11.7% for PD-derived pericytes). With time, at day 14, the proportion of control and PD-derived cells without aggregates increased (53.3% and 53.6%, respectively; Fig 5B).

The density plots observed for Fibrils and fibrils91 followed that of Ribbons, whereas fibrils65 were similar to fibrils110 (S2 Fig). Fluorescent debris was picked up in the untreated control and gradually increased with time (0h-14 days; 5 to 10% of control, 15–16% PD-derived pericytes) and peaked at 21 days (20% and 36%, respectively) (S2A–S2D Fig). Overall, both average counts/cell and aggregate size/cell decreased over time, indicating that the fewer remaining cells contain fewer and smaller aggregates. Aggregates remained visible at the latest timepoints, with many pericytes still containing aggregated α-syn 21 days after exposure (Figs 5 and S2A–S2D).
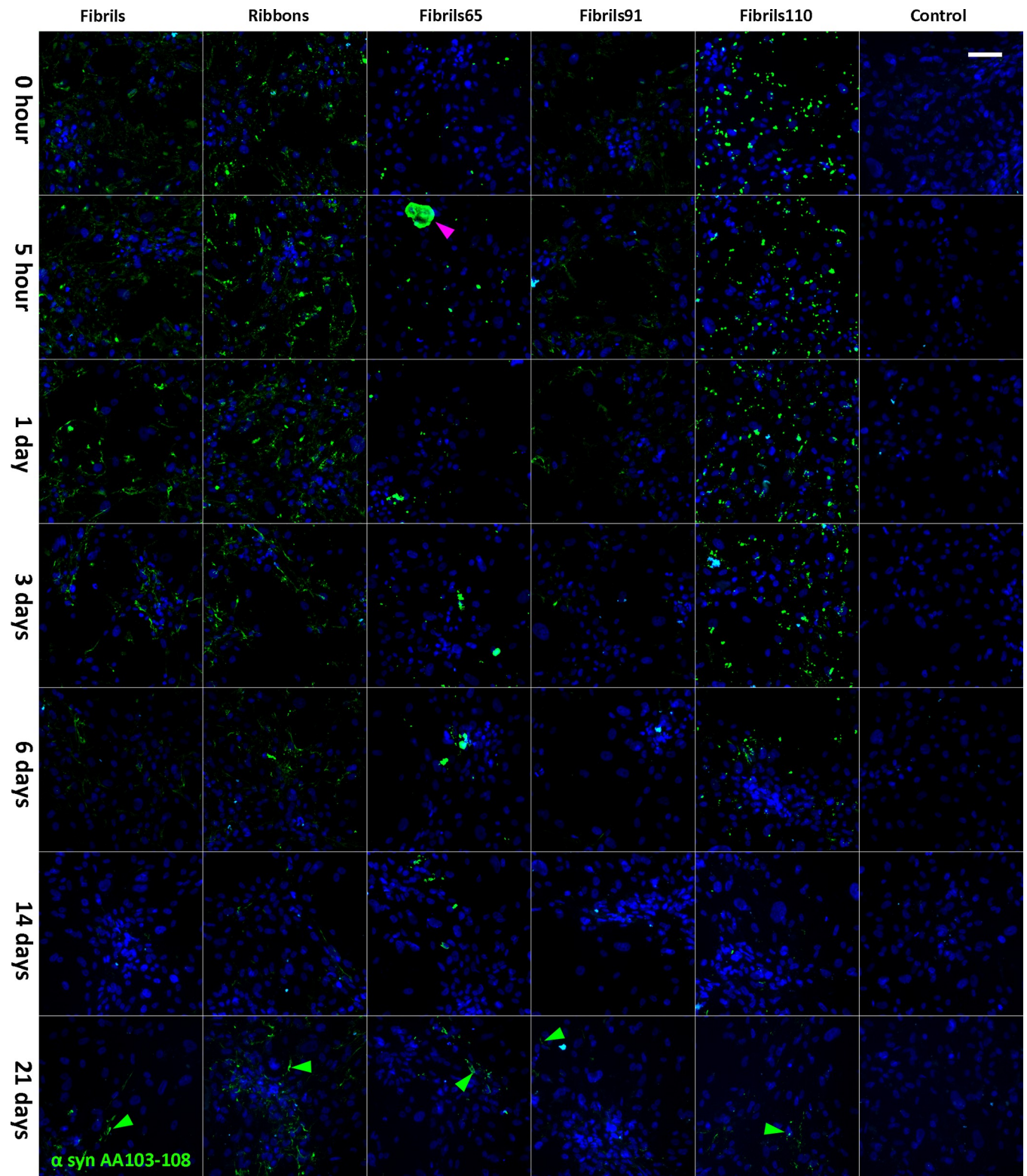
Fig 3. Immunofluorescent labelling of α-syn strains in pericytes with α-syn specific antibodies AA103-108 (green) after pre-treatment with 100nM Fibrils, Ribbons, fibrils65, fibrils91 and fibrils110. Large aggregates were occasionally found for fibrils65 (magenta arrow). The scale bar represents 100 μm.

https://doi.org/10.1371/journal.pone.0277658.g003
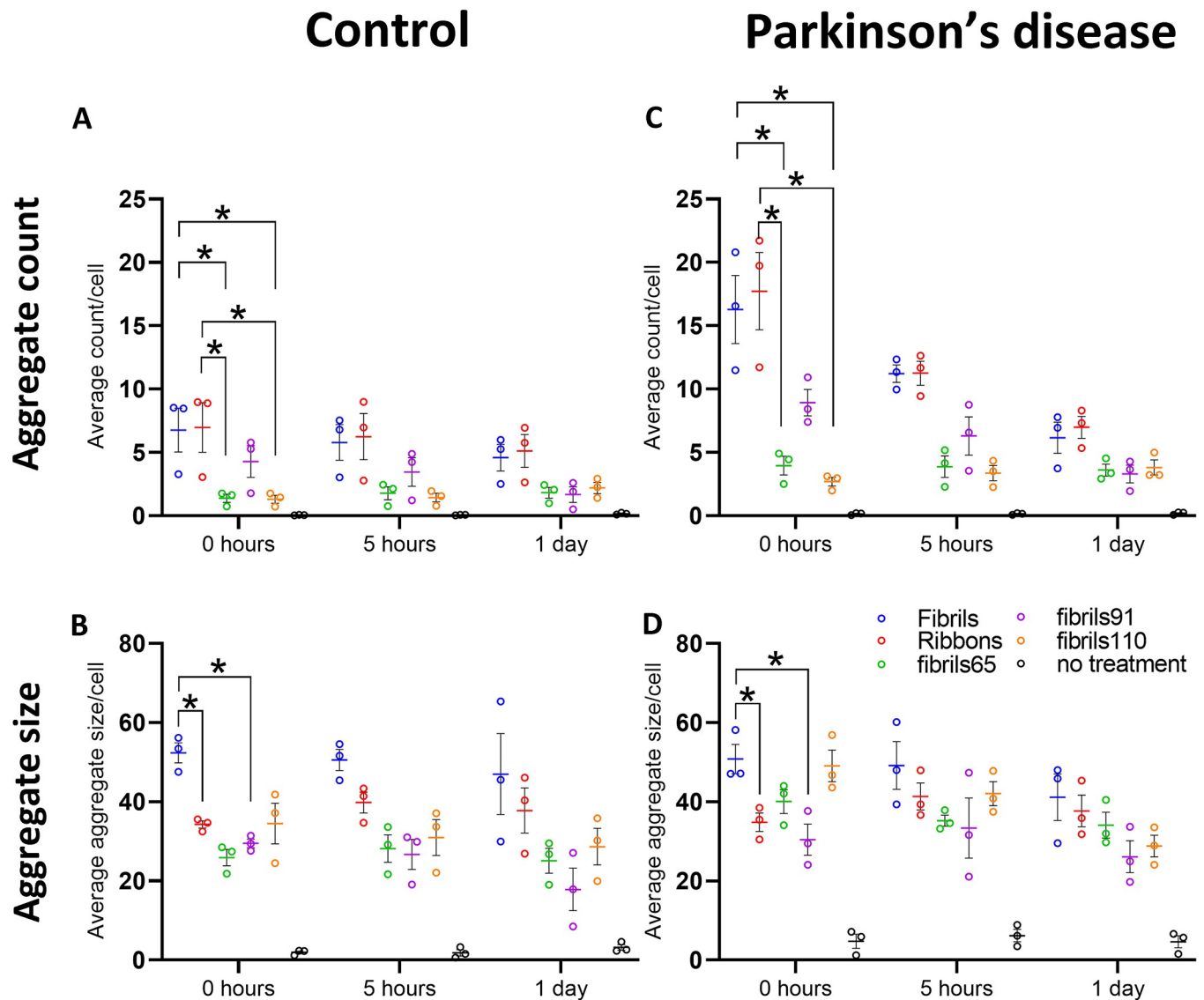
Control

Parkinson's disease

Fig 4. Strain-specific differences in control and PD-derived post-mortem pericytes. (A-B) Average aggregate count/cell analysis and (C-D) average aggregate size/cell analysis based on AA103-108 for control pericytes (n = 3) and PD pericytes (n = 3). Two-way ANOVA was used with Tukey's post hoc adjustment for multiple comparisons. An asterisk indicates significant differences in control and PD-derived post-mortem pericytes * (p<0.05).

https://doi.org/10.1371/journal.pone.0277658.g004

Sustained α-syn internalisation by pericytes in human primary mixed neuronal cultures

Differences may exist between uptake and clearance of α-syn in a monoculture and mixed cell populations. Indeed, pericytes might no longer internalise α-syn aggregate in the presence of other cell types. To show uptake, we added fluorescently labelled α-syn Fibrils for 60 hours to primary cell cultures consisting of mature human primary neurons, astrocytes, microglia (red arrow) and pericytes (yellow arrow). These neurons' neurochemical phenotype and functionality have been extensively validated [30,35]. The average age of donors for the mixed neuronal cell cultures in this study was (30.5 ± Seven years). One cell type displayed intense labelling (red) indicative of rapid binding and internalisation of α-syn fibrils from the culture media (red arrow, Fig 6A, S6 Movie). These cells are CD45+/Iba1+ microglia that rapidly internalised
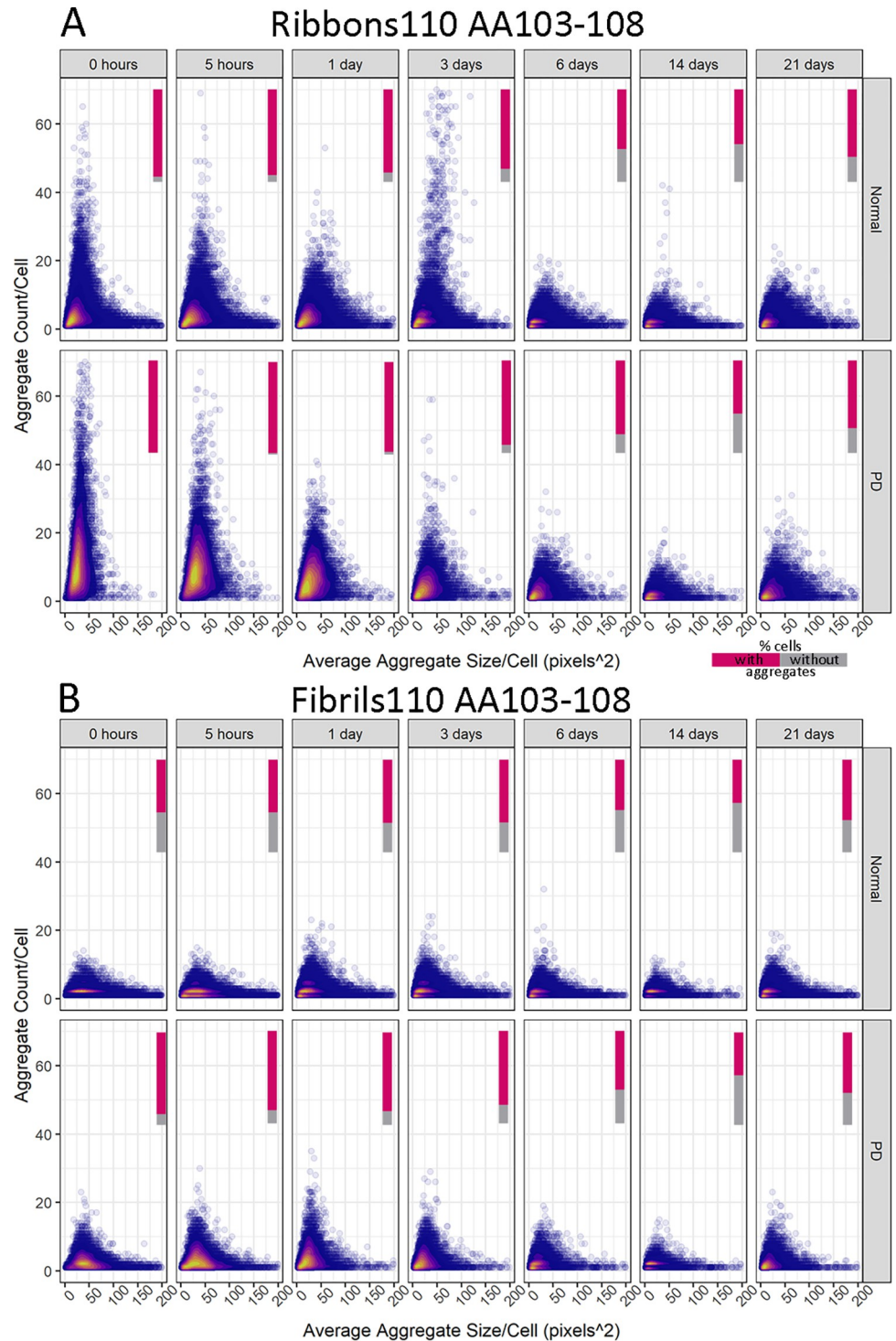
Fig 5. Density plots showing a differential response to α-syn aggregates for control and PD-derived pericytes based on AA103-108 for Ribbons and fibrils 110. Cells without aggregates are excluded from density plots. Relative amounts of cells with aggregates are represented in a bar (% cells with aggregates in magenta, % cells without aggregates in grey).
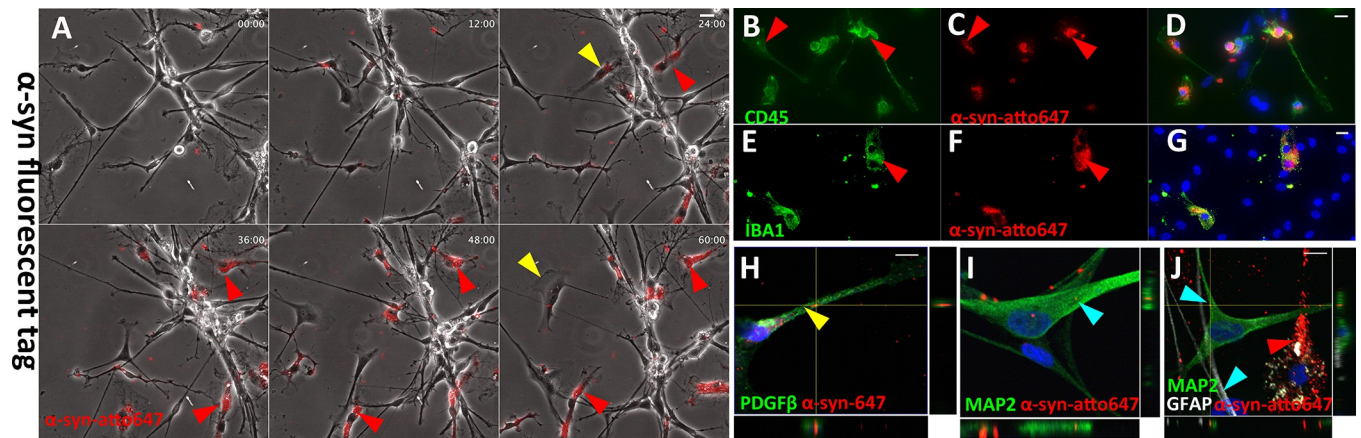
https://doi.org/10.1371/journal.pone.0277658.g005

Fig 6. Primary human mixed neuronal cell exposed to α-syn aggregates—internalisation is cell type-specific. (A) Representative images of live cell recording with α-syn-594 aggregates. (B-C) Confocal imaging indicates that α-syn-594 aggregates are present within neurons and pericytes. (E-I) Cells with high α-syn aggregate load are microglia CD45^{+} and IBA1^{+}. Representative images of primary human mixed neuronal cell exposed to (J) Ribbons with (L-O) Ribbons within Astrocytes GFAP high, MAP2 low and (P-S) neurons GFAP low-MAP2 high.

α-syn (red arrows Fig 6B–6G). The proximity of microglia did not prevent α-syn fibrils internalisation by PDGFRβ[+] pericytes (yellow arrow, Fig 6H, S6 Movie). Within the timeframe (96 hours), MAP2^{+} neurons (blue arrow, Fig 6I) internalised α-syn fibrils to a much lesser extent. Confocal imaging with orthogonal projection demonstrates the difference in α-syn fibrils internalisation between microglia (red arrow) and neurons (blue arrow) visible (Fig 6J). These co-culture experiments revealed that pericytes in mixed cell populations retain their capacity to internalise fibrillar α-syn aggregates.

Discussion

Situated at the blood and the brain parenchyma interface, pericytes are essential in regulating blood-brain barrier function and as mediators of neuroinflammation [17,39]. In PD, decreased pericyte coverage of vessels is coupled with increased leakiness of the blood-brain barrier [20,21]. Our previous work showed that *in situ* human brain pericytes contain a similar amount of α-syn aggregates as microglia and astrocytes [13]. Furthermore, primary human pericytes can transfer α-syn through nanotubes *in vitro* to neighbouring cells [24]. It remains unclear whether pericytes function as a mere conduit for α-syn spread or if they are also involved in aggregate seeding. Pericytes have either low or no endogenous expression of α-syn, suggesting seeding in a pure pericyte culture is unlikely. We, therefore, hypothesise that pericytes must internalise α-syn if they are involved in aggregate seeding. Here, we demonstrate that pericytes efficiently internalise fibrillar α-syn and efficiently break down α-syn aggregates in vitro. Uptake and clearance are observed for all α-syn aggregates (Fibrils, Ribbons, fibrils65, fibrils91 and fibrils110) analysed in this study. As such, pericytes could, together with microglia and astrocytes, act as barriers that remove α-syn aggregates, thereby reducing α-syn-induced toxicity and slowing down spread, in turn delaying disease onset.

It is well-established that in synucleinopathies, Lewy body pathology spreads throughout the central nervous system in disease-specific patterns [4]. α-syn is a constitutive component of Lewy bodies and neurites and is known to aggregate into large fibrillar assemblies [40]. Once a cell contains aberrant α-syn, there are three potential outcomes: degradation, deposition in a specialised compartment (inclusion), or release into the extracellular space. Upon

release, α-syn can be taken up by acceptor cells where the cycle of protein aggregation in a prion-like manner continues or degradation occurs. Compared to astrocytes and microglia, pericytes are not well-studied in this aspect. Different brain cells take up exogenous α-syn with different kinetics [41]. Microglia are more efficient than neurons and astrocytes in the uptake and degradation of extracellular α-syn [41,42]. This suggests that the uptake pathways are differentially regulated or that different cell types are equipped with distinct receptors for extracellular α-syn [42]. Such interaction with fibrillar α-syn is likely influenced in mixed cell cultures. Therefore, we demonstrate that pericytes internalise α-syn both in monoculture and when combined with other cell types known to phagocytose α-syn [14,41,43]. In both culture conditions, pericytes efficiently take up fibrillar α-syn. Uptake by pericytes still occurred despite the proximity of professional phagocytes like microglia, strengthening the results obtained from our pericyte monoculture.

Specific cleavage of α-syn by pericytes has not been previously studied. In this study, using different epitope-specific α-syn antibodies directed at the α-syn C-terminus, we show that human primary pericytes can efficiently degrade α-syn aggregates through cleavage into several smaller fragments. These fragments were previously observed in the BV-2 microglial cell line, primary murine microglia, astrocytes and SH-SY5Y cells [14,41,44]. Truncated α-syn is consistently found in human brain tissue; AA1-119 (truncated at Asp-119) and AA1-122 (truncated at Asn-122) have an abundance as high as 20–25% relative to full-length α-syn [45,46]. Degradation of α-syn can occur via autophagic clearance and proteasomal degradation, and the dysfunction of both systems is linked to PD pathogenesis [47–50]. Recent work from our group shows that degradation of α-syn aggregates in pericytes occurs through the lysosomal pathway [51]. PD pericytes contain a higher number of lysosomes compared to healthy control pericytes. However, lysosomes from PD pericytes are less effective at degrading aggregated α-syn, indicating that the marked increase of lysosomes compensates for an impaired lysosomal degradation [51].

In this study, we determined that the number, aggregate size and ongoing detection of fibrillar α-syn in pericytes varies at the early time points. PD pericytes showed an increased variation in our measurements. This could be caused by the gradual loss of pericytes that is not uniform but affects every capillary differently. As such, it is possible that individual pericytes derived from PD have different characteristics influencing degradation, which could explain the higher variability seen within PD pericytes [52,53]. Although this comparison is potentially affected by differences in PMD and age at death, it shows that irrespective of these variables, all pericytes (control and PD derived) degrade α-syn aggregates to the same levels (less than 2–3 aggregates/cell). Pericytes exposed to Fibrils and Ribbons have high aggregate counts, whereas fibrils65 and fibrils110 have a limited number of aggregates per cell. We show that all α-syn aggregates are degraded by pericytes but cleaved α-syn species remain present for at least 21 days. Based on our data, we speculate that fibrils65 and fibrils110 are internalised at a slower rate, which would explain the lower number of aggregates/cell for these strain types. It is hard to speculate the exact contribution of internalisation versus processing and secretion. All factors likely play a role in the clearance of fibrillar α-syn by pericytes.

Unique to this study is the prolonged timeframe (21 days post-exposure) that pericytes were followed. This prolonged follow-up period showed that cleavage occurs early after exposure but that cleaved α-syn fragments remain present within pericytes for several weeks. It is important to highlight that the proportion of cells (17–59%) containing primarily cleaved α-syn at the later timepoints (14–21 days) can be relatively high depending on the strain type. α-syn cleavage is positively correlated with accelerated aggregation and pathology in cell and mouse models [36–38]. Even though we did not investigate α-syn in the culture media in this study, a proportion of the aggregates is likely secreted by the pericytes. Furthermore, the

spreading of remnant α-syn fragments through secretion, tunnelling nanotubes or endosomal vesicles to neighbouring cells, as seen in microglia, is also possible [3,15,24,43,54]. Although these mechanisms are believed to dilute the burden over multiple cells [15], when exposure exceeds breakdown capacity, they may also contribute to the prolonged presence of incompletely processed α-syn aggregates that possess seeding propensity, given that they retain their amyloid core. Indeed, all structural studies have demonstrated that the C-terminal end of α-syn spanning residues 100 to 140 is mostly dynamic with little contribution to the fibrils amyloid core.

Conclusion

Our data suggest that cleaved α-syn remains present for prolonged periods adding to the current literature that insufficient degradation caused by high aggregated α-syn load could potentially favour propagation. Furthermore, pericytes could play an integral part in degrading α-syn aggregates within the brain, irrespective of strain. As such, pericytes are a potential new target to reduce α-syn-induced toxicity, slow the spread and delay disease onset.

Supporting information

S1 Fig. Immunofluorescent labelling of endogenous, monomeric or fibrillar fibrils treated pericytes. No α-syn puncta detected with α-syn specific antibodies AA103-108 (green) after treatment with monomeric α-syn (100μM and 500μM) (A). Immunofluorescent labelling of endogenous, monomeric or fibrillar α-syn treated pericytes with α-syn specific antibodies AA103-108 (green), PDGFRβ (red) and α-syn Phospho S129 (magenta) after 4 hour pre-treatment with 100nM Fibrils or monomeric α-syn (2 days, B; 10 days C). Scale bars represent 20 μm.
(TIF)

S2 Fig. Density plots of showing a differential response to α-syn aggregates between control and PD-derived pericytes based on AA103-108 for Fibrils, fibrils65, fibrils 91 no treatment control. Cells without aggregates are excluded from density plots. Relative amounts of cells with aggregates represented in bar (% cells with aggregates in magenta, % cells without aggregates in grey). The colours represent a 2D kernel density estimation. It is scaled to 1 for each graph, with the bright yellow area displaying the highest density of cells.
(TIF)

S1 Raw images. Full western blots for Fibrils, Ribbons, fibrils65, fibrils91, fibrils110 and no treatment control with AA103-108, AA124-134 and GAPDH. Two blots used for each alpha synuclein strain. Each blot was labelled with α-syn antibodies (AA103-108 or AA124-134), imaged, stripped and relabelled for GAPDH.
(PDF)

S1 Movie. Life cell imaging (120 hours) of pericytes pre-treated for 4 hours with 100nM Fibrils-atto647.
(AVI)

S2 Movie. Life cell imaging (120 hours) of pericytes pre-treated for 4 hours with 100nM Ribbons-atto647.
(AVI)

S3 Movie. Life cell imaging (120 hours) of pericytes pre-treated for 4 hours with 100nM fibrils65-atto647.
(AVI)

S4 Movie. Life cell imaging (72 hours) of pericytes pre-treated for 4 hours with 100nM fibrils91-atto647.
(AVI)

S5 Movie. Life cell imaging (90 hours) of pericytes pre-treated for 4 hours with 100nM fibrils110-atto647.
(AVI)

S6 Movie. Life cell imaging (90 hours) of mixed neuronal cell cultures pre-treated for 4 hours with 100nM fibrils110-atto647.
(AVI)

S7 Movie. Life cell imaging showing α-syn uptake by pericyte adjacent to microglia.
(AVI)

S1 File. Supplementary M&M 1 R script used for image analysis.
(DOCX)

Author Contributions

Conceptualization: Birger Victor Dieriks, Ronald Melki, Mike Dragunow.

Data curation: Birger Victor Dieriks, Blake Highet, Ronald Melki.

Formal analysis: Birger Victor Dieriks, Blake Highet.

Funding acquisition: Birger Victor Dieriks, Ronald Melki, Maurice A. Curtis, Mike Dragunow.

Investigation: Birger Victor Dieriks, Taylor J. Stevenson, Victoria Low, Thomas I-H Park.

Methodology: Birger Victor Dieriks, Victoria Low, Ronald Melki.

Project administration: Birger Victor Dieriks, Mike Dragunow.

Resources: Ania Alik, Tracy Bellande, Thomas I-H Park, Jason Correia, Patrick Schweder, Richard L. M. Faull, Ronald Melki, Maurice A. Curtis, Mike Dragunow.

Supervision: Ronald Melki, Maurice A. Curtis, Mike Dragunow.

Validation: Birger Victor Dieriks.

Visualization: Birger Victor Dieriks, Blake Highet.

Writing – original draft: Birger Victor Dieriks, Blake Highet, Ronald Melki, Mike Dragunow.

Writing – review & editing: Birger Victor Dieriks, Blake Highet, Taylor J. Stevenson, Maurice A. Curtis, Mike Dragunow.

References

1. Villar-Piqué A, Lopes da Fonseca T, Outeiro TF. Structure, function and toxicity of alpha-synuclein: the Bermuda triangle in synucleinopathies. J Neurochem. 2016; 139:240–55. https://doi.org/10.1111/jnc.13249 PMID: 26190401

2. Malmberg M, Malm T, Gustafsson O, Sturchio A, Graff C, Espay AJ, et al. Disentangling the Amyloid Pathways: A Mechanistic Approach to Etiology. Front Neurosci. 2020; 14(April):1–11. https://doi.org/10.3389/fnins.2020.00256 PMID: 32372895

3. Stefanis L, Emmanouilidou E, Pantazopoulou M, Kirik D, Vekrellis K, Tofaris GK. How is alpha-synuclein cleared from the cell? J Neurochem. 2019; 150(5):577–90. https://doi.org/10.1111/jnc.14704 PMID: 31069800

4. Braak H, Tredici K del, Rüb U, de Vos RAI, Jansen Steur ENH, Braak E. Staging of brain pathology related to sporadic Parkinson's disease. Neurobiol Aging. 2003; 24(2):197–211. https://doi.org/10.1016/s0197-4580(02)00065-9 PMID: 12498954

5. Tran J, Anastacio H, Bardy C. Genetic predispositions of Parkinson's disease revealed in patient-derived brain cells. NPJ Parkinsons Dis. 2020; 6(1). https://doi.org/10.1038/s41531-020-0110-8 PMID: 32352027

6. Hoppe SO, Uzunoğlu G, Nussbaum-Krammer C. α-Synuclein Strains: Does Amyloid Conformation Explain the Heterogeneity of Synucleinopathies? Biomolecules. 2021; 11(7). https://doi.org/10.3390/biom11070931 PMID: 34201558

7. van der Perren A, Gelders G, Fenyi A, Bousset L, Brito F, Peelaerts W, et al. The structural differences between patient-derived α-synuclein strains dictate characteristics of Parkinson's disease, multiple system atrophy and dementia with Lewy bodies. Acta Neuropathol. 2020; 139(6):977–1000. https://doi.org/10.1007/s00401-020-02157-3 PMID: 32356200

8. Peelaerts W, Bousset L, van der Perren A, Moskalyuk A, Pulizzi R, Giugliano M, et al. α-Synuclein strains cause distinct synucleinopathies after local and systemic administration. Nature. 2015; 522 (7556):340–4. https://doi.org/10.1038/nature14547 PMID: 26061766

9. Lau A, So RWL, Lau HHC, Sang JC, Ruiz-Riquelme A, Fleck SC, et al. α-Synuclein strains target distinct brain regions and cell types. Nat Neurosci. 2020; 23(1):21–31. https://doi.org/10.1038/s41593-019-0541-x PMID: 31792467

10. Liu D, Guo J, Su J, Svanbergsson A, Yuan L, Haikal C, et al. Differential seeding and propagating efficiency of α-synuclein strains generated in different conditions. Transl Neurodegener. 2021; 10(20):1–15. https://doi.org/10.1186/s40035-021-00242-5 PMID: 34148543

11. Sorrentino ZA, Giasson BI, Chakrabarty P. α-Synuclein and astrocytes: tracing the pathways from homeostasis to neurodegeneration in Lewy body disease. Acta Neuropathol. 2019; 138(1):1–21. https://doi.org/10.1007/s00401-019-01977-2 PMID: 30798354

12. Tanriöver G, Bacioglu M, Schweighauser M, Mahler J, Wegenast-Braun BM, Skodras A, et al. Prominent microglial inclusions in transgenic mouse models of α-synucleinopathy that are distinct from neuronal lesions. Acta Neuropathol Commun. 2020; 8(1):1–11.

13. Stevenson TJ, Murray HC, Turner C, Faull RLM, Dieriks BV, Curtis MA. α-synuclein inclusions are abundant in non-neuronal cells in the anterior olfactory nucleus of the Parkinson's disease olfactory bulb. Sci Rep. 2020;1–10.

14. Loria F, Vargas JY, Bousset L, Syan S, Salles A, Melki R, et al. α-Synuclein transfer between neurons and astrocytes indicates that astrocytes play a role in degradation rather than in spreading. Acta Neuropathol. 2017 Jul;1–20. https://doi.org/10.1007/s00401-017-1746-2 PMID: 28725967

15. Scheiblich H, Dansokho C, Mercan D, Schmidt S v., Bousset L, Wischhof L, et al. Microglia jointly degrade fibrillar alpha-synuclein cargo by distribution through tunneling nanotubes. Cell. 2021; 184 (20):5089–5106.e21. https://doi.org/10.1016/j.cell.2021.09.007 PMID: 34555357

16. Russ K, Teku G, Bousset L, Redeker V, Piel S, Savchenko E, et al. TNF-α and α-synuclein fibrils differently regulate human astrocyte immune reactivity and impair mitochondrial respiration. Cell Rep. 2021; 34(12):108895. https://doi.org/10.1016/j.celrep.2021.108895 PMID: 33761362

17. Rustenhoven J, Jansson D, Smyth LC, Dragunow M. Brain Pericytes As Mediators of Neuroinflammation. Trends Pharmacol Sci. 2017; 38(3):291–304. https://doi.org/10.1016/j.tips.2016.12.001 PMID: 28017362

18. Jansson D, Rustenhoven J, Feng S, Hurley D, Oldfield RL, Bergin PS, et al. A role for human brain pericytes in neuroinflammation. J Neuroinflammation. 2014; 11:104. https://doi.org/10.1186/1742-2094-11-104 PMID: 24920309

19. Rustenhoven J, Scotter EL, Jansson D, Kho DT, Oldfield RL, Bergin PS, et al. An anti-inflammatory role for C/EBPδ in human brain pericytes. Sci Rep. 2015; 5:12132. https://doi.org/10.1038/srep12132 PMID: 26166618

20. Gray MT, Woulfe JM. Striatal blood-brain barrier permeability in Parkinson's disease. Journal of Cerebral Blood Flow and Metabolism. 2015; 35(5):747–50. https://doi.org/10.1038/jcbfm.2015.32 PMID: 25757748

21. Yang P, Waldvogel HJ, Faull RLM, Dragunow M, Guan J. Vascular degeneration in Parkinson 's disease. Alzheimer's and Parkinson's Disease. 2016; 2(1).

22. Rostami J, Holmqvist S, Lindström V, Sigvardson J, Westermark GT, Ingelsson M, et al. Human astrocytes transfer aggregated alpha-synuclein via tunneling nanotubes. Journal of Neuroscience. 2017; 37 (49):11835–53. https://doi.org/10.1523/JNEUROSCI.0983-17.2017 PMID: 29089438

23. Abounit S, Bousset L, Loria F, Zhu S, de Chaumont F, Pieri L, et al. Tunneling nanotubes spread fibrillar α-synuclein by intercellular trafficking of lysosomes. EMBO J. 2016 Oct; 35(19):2120–38. https://doi.org/10.15252/embj.201593411 PMID: 27550960

24. Dieriks BV, Park TI-H, Fourie C, Faull RLM, Dragunow M, Curtis MA. α-synuclein transfer through tunneling nanotubes occurs in SH-SY5Y cells and primary brain pericytes from Parkinson's disease patients. Sci Rep. 2017 Feb; 7:42984. https://doi.org/10.1038/srep42984 PMID: 28230073

25. Ghee M, Melki R, Michot N, Mallet J. PA700, the regulatory complex of the 26S proteasome, interferes with α-synuclein assembly. FEBS J. 2005; 272(16):4023–33.

26. Bousset L, Pieri L, Ruiz-Arlandis G, Gath J, Jensen PH, Habenstein B, et al. Structural and functional characterization of two alpha-synuclein strains. Nat Commun. 2013; 4(2575). https://doi.org/10.1038/ncomms3575 PMID: 24108358

27. Makky A, Bousset L, Polesel-Maris J, Melki R. Nanomechanical properties of distinct fibrillar polymorphs of the protein α-synuclein. Sci Rep. 2016; 6:1–10.

28. Pieri L, Madiona K, Melki R. Structural and functional properties of prefibrillar α-synuclein oligomers. Sci Rep. 2016; 6(April):1–15. https://doi.org/10.1038/srep24526 PMID: 27075649

29. Grozdanov V, Bousset L, Hoffmeister M, Bliederhaeuser C, Meier C, Madiona K, et al. Increased Immune Activation by Pathologic α-Synuclein in Parkinson's Disease. Ann Neurol. 2019; 86(4):593–606. https://doi.org/10.1002/ana.25557 PMID: 31343083

30. Park TIH, Smyth LCD, Aalderink M, Woolf ZR, Rustenhoven J, Lee K, et al. Routine culture and study of adult human brain cells from neurosurgical specimens. Nat Protoc. 2022; 17(2):190–221. https://doi.org/10.1038/s41596-021-00637-8 PMID: 35022619

31. Smyth LCD, Rustenhoven J, Scotter EL, Schweder P, Faull RLM, Park TIH, et al. Markers for human brain pericytes and smooth muscle cells. J Chem Neuroanat. 2018; 92(January):48–60. https://doi.org/10.1016/j.jchemneu.2018.06.001 PMID: 29885791

32. Rustenhoven J, Aalderink M, Scotter EL, Oldfield RL, Bergin PS, Mee EW, et al. TGF-beta1 regulates human brain pericyte inflammatory processes involved in neurovasculature function. J Neuroinflammation. 2016; 13(1):1–15. https://doi.org/10.1186/s12974-016-0503-0 PMID: 26867675

33. Rustenhoven J, Smyth LC, Jansson D, Schweder P, Aalderink M, Scotter EL, et al. Modelling physiological and pathological conditions to study pericyte biology in brain function and dysfunction. BMC Neurosci. 2018; 19(1):1–15.

34. Smyth LCD, Rustenhoven J, Park TI-H, Schweder P, Jansson D, Heppner PA, et al. Unique and shared inflammatory profiles of human brain endothelia and pericytes. J Neuroinflammation. 2018; 15(1):138. https://doi.org/10.1186/s12974-018-1167-8 PMID: 29751771

35. Park TI-H, Schweder P, Lee K, Dieriks B v, Jung Y, Smyth L, et al. Isolation and culture of functional adult human neurons from neurosurgical brain specimens. Brain Commun. 2020; 2(2). https://doi.org/10.1093/braincomms/fcaa171 PMID: 33215086

36. Waldvogel HJ, Curtis MA, Baer K, Rees MI, Faull RL. Immunohistochemical staining of post-mortem adult human brain sections. Nat Protoc. 2006; 1(6):2719–32. https://doi.org/10.1038/nprot.2006.354 PMID: 17406528

37. Highet B, Dieriks BV, Murray HC, Faull RLM, Curtis MA. Huntingtin aggregates in the olfactory bulb in Huntington's disease. Front Aging Neurosci. 2020; 12:261. https://doi.org/10.3389/fnagi.2020.00261 PMID: 33013352

38. Shrivastava AN, Bousset L, Renner M, Redeker V, Savistchenko J, Triller A, et al. Differential Membrane Binding and Seeding of Distinct α-Synuclein Fibrillar Polymorphs. Biophys J. 2020; 118(6):1301–20. https://doi.org/10.1016/j.bpj.2020.01.022 PMID: 32059758

39. Duan L, Zhang X-D, Miao W-Y, Sun Y-J, Xiong G, Wu Q, et al. PDGFRβ Cells Rapidly Relay Inflammatory Signal from the Circulatory System to Neurons via Chemokine CCL2. Neuron. 2018; 100(1):183–200.e8. https://doi.org/10.1016/j.neuron.2018.08.030 PMID: 30269986

40. Shahmoradian SH, Lewis AJ, Genoud C, Hench J, Moors TE, Navarro PP, et al. Lewy pathology in Parkinson's disease consists of crowded organelles and lipid membranes. Nat Neurosci. 2019; 22 (7):1099–109. https://doi.org/10.1038/s41593-019-0423-2 PMID: 31235907

41. Lee HJ, Suk JE, Bae EJ, Lee SJ. Clearance and deposition of extracellular α-synuclein aggregates in microglia. Biochem Biophys Res Commun. 2008; 372(3):423–8.

42. Grozdanov V, Danzer KM. Release and uptake of pathologic alpha-synuclein. Cell Tissue Res. 2018; 373(1):175–82. https://doi.org/10.1007/s00441-017-2775-9 PMID: 29411106

43. Xia Y, Zhang G, Kou L, Yin S, Han C, Hu J, et al. Reactive microglia enhance the transmission of exosomal α-synuclein via toll-like receptor 2. Brain. 2021; 144(7):2024–37. https://doi.org/10.1093/brain/awab122 PMID: 33792662

44. Pieri L, Chafey P, le Gall M, Clary G, Melki R, Redeker V. Cellular response of human neuroblastoma cells to α-synuclein fibrils, the main constituent of Lewy bodies. Biochimica et Biophysica Acta (BBA)-General Subjects. 2016; 1860(1):8–19. https://doi.org/10.1016/j.bbagen.2015.10.007 PMID: 26468903

45. Moors TE, Maat CA, Niedieker D, Mona D, Petersen D, Timmermans-Huisman E, et al. Subcellular orchestration of alpha-synuclein variants in Parkinson's disease brains revealed by 3D multicolor STED microscopy. bioRxiv. 2018 https://doi.org/10.1101/470476

46. Sorrentino ZA, Giasson BI. The emerging role of α-synuclein truncation in aggregation and disease. Journal of Biological Chemistry. 2020; 295(30):10224–44. https://doi.org/10.1074/jbc.REV120.011743 PMID: 32424039

47. Cuervo AM. Impaired Degradation of Mutant -Synuclein by Chaperone-Mediated Autophagy. Science (1979). 2004 Aug; 305(5688):1292–5.

48. Emmanouilidou E, Stefanis L, Vekrellis K. Cell-produced α-synuclein oligomers are targeted to, and impair, the 26S proteasome. Neurobiol Aging. 2010 https://doi.org/10.1016/j.neurobiolaging.2008.07.008 PMID: 18715677

49. Dargemont C, Ossareh-Nazari B. Cdc48/p97, a key actor in the interplay between autophagy and ubiquitin/proteasome catabolic pathways. Biochim Biophys Acta Mol Cell Res. 2012; 1823(1):138–44. https://doi.org/10.1016/j.bbamcr.2011.07.011 PMID: 21807033

50. Xilouri M, Brekk OR, Stefanis L. α-Synuclein and protein degradation systems: a reciprocal relationship. Mol Neurobiol. 2013 https://doi.org/10.1007/s12035-012-8341-2 PMID: 22941029

51. Stevenson TJ, Johnson R, Savistchenko J, Rustenhoven J, Woolf Z, Smyth LCD, et al. Pericytes take up and degrade α-synuclein but succumb to apoptosis under cellular stress. Sci Rep. 2022; 12(17314). https://doi.org/10.1038/s41598-022-20261-0 PMID: 36243723

52. Stancu IC, Cremers N, Vanrusselt H, Couturier J, Vanoosthuyse A, Kessels S, et al. Aggregated Tau activates NLRP3–ASC inflammasome exacerbating exogenously seeded and non-exogenously seeded Tau pathology in vivo. Acta Neuropathol. 2019; 137(4):599–617. https://doi.org/10.1007/s00401-018-01957-y PMID: 30721409

53. Leng F, Edison P. Neuroinflammation and microglial activation in Alzheimer disease: where do we go from here? Nat Rev Neurol. 2021; 17(3):157–72. https://doi.org/10.1038/s41582-020-00435-y PMID: 33318676

54. Alarcon-Martinez L, Villafranca-Baughman D, Quintero H, Kacerovsky JB, Dotigny F, Murai KK, et al. Interpericyte tunnelling nanotubes regulate neurovascular coupling. Nature. 2020; 585(7823):91–5. https://doi.org/10.1038/s41586-020-2589-x PMID: 32788726